Propulsion and Power Research 2022;11(2):196–208

http://ppr.buaa.edu.cn/

Propulsion and Power Research

www.sciencedirect.com

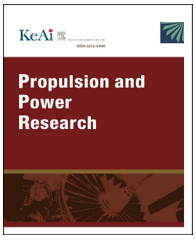

ORIGINAL ARTICLE

Effects of propeller load fluctuations on performance and emission of a lean-burn natural gas engine at part-load conditions

S. Tavakoli[a,b,*], **J. Schramm**[b], **E. Pedersen**[a]

[a]*Department of Marine Technology, Norwegian University of Science and Technology, Trondheim, Norway*
[b]*Department of Mechanical Engineering, Technical University of Denmark, Lyngby, Denmark*

Received 29 September 2020; accepted 13 April 2022
Available online 21 June 2022

KEYWORDS

Lean-burn combustion;
Emission formation;
Methane slip;
NO_X;
Part-load operation

Abstract Providing stable combustion of lean-burn natural gas engines was always a big challenge, particularly during a low load operation. In transient sea conditions, there is an additional concern due to irregular time-varying loads. Therefore, this study aimed at investigating the part-load operation of a marine spark-ignition lean-burn natural gas engine by simulating the entire engine. The engine's essential components are modeled, including air manifold, intake valves, fuel system, controllers, combustion chamber, exhaust valves, exhaust manifold and turbocharger.

In steady-state, the results of emission compounds from modeling have been compared to measured data from 25% to 100% loads. For transient conditions, for the sample time of about 50 min, the fuel flow and turbocharger output are selected from the vessel logged data and compared with the simulation results. The model has shown the great potential of predicting the engine response throughout the steady-state and transient conditions. Simulating the engine at part-load transient condition showed that the unburned hydrocarbon formation, known as methane slip in lean-burn gas engines, is more than the part-load steady-state. This increase of methane slip is due to the combustion instability in lower loads and flame extinguishing in such transient conditions. The engine measured data shows a double amount of methane slip in a 25% load than the 100% load in steady-state. However, the simulation output in the

*Corresponding author.
E-mail address: sadi.tavakoli@ntnu.no (S. Tavakoli).
Peer review under responsibility of Propulsion and Power Research.

ELSEVIER | Production and Hosting by Elsevier on behalf of KeAi

https://doi.org/10.1016/j.jppr.2022.04.001

transient conditions confirms an increase in methane slip over four times than equivalent steady-state load. Moreover, the lean-burn gas engine releases less NO_X in part-load operation in a steady-state due to lower in-cylinder temperature. In transient conditions, there is remarkable instability in excess air ratio. Due to this instability, there is a rich mixture in instantaneous time steps during loads up. Therefore, it will result in an unusually high amount of NO_X, and more than two times in comparison with the equivalent steady-state output.

Nomenclature

$\dot{m}$	mass flux
A	cross-sectional flow area
A_e	flame front area
A_S	heat transfer surface area
D	diameter
DF	dual fuel
E_A	activation energy
EVO	exhaust valve opening
GWP	global warming potential
H	hydrogen
h	total specific enthalpy
h_c	heat transfer coefficient
IVC	intake valve closing
K_P	pressure loss coefficient
M	mass
N	speed
NO	nitrogen oxide
P	pressure
R_K	post-oxidation rate
R_S	fuel burn rate
S_L	laminar flame speed
S_T	turbulent flame speed
T	temperature
t	time
u	velocity at the boundary
UHC	unburned hydrocarbon
V	volume
BMEP	brake mean effective pressure
CO	carbon monoxide
CO_2	carbon dioxide
EGR	exhaust gas recirculation
GHG	greenhouse gas
IMO	international maritime organization
PID	proportional-integral-derivative
PM	particulate matter
PTI	power take-in
PTO	power take-off
Re_t	turbulent Reynolds number
rpm	revolutions per minute
SO_X	sulfur oxides
VTG	variable turbine geometry

Greek letters

φ	equivalence ratio
ρ	density

1. Introduction

The importance of natural gas as a hydrocarbon-based fuel for engines in marine applications is increasing continuously due to the high thermal efficiency of burning natural gas in a very lean mixture in lean-burn natural gas engines.

In addition, during recent years, the International Maritime Organization (IMO) applied a maximum specified nitrogen oxide (NO_X) and sulfur oxides (SO_X) in various regulations [1]. It has also defined an initial strategy on reducing greenhouse gas (GHG) emissions from ships by achieving net-zero GHG emissions from shipping by the end of the 21st century by:

- Reducing total annual by at least 50% by 2050 compared to 2008,
- Reducing carbon dioxide (CO_2) emissions intensity per transport by at least 40% by 2030, and by at least 70% by 2050.

Natural gas engines produce four main emissions: NO_X, CO_2, carbon monoxide (CO) and unburned hydrocarbon (UHC), which is mainly methane [2]. Natural gas contributes to relatively low particulate matter (PM) and zero SO_X [3]. Lean-burn spark-ignition gas engines with lambda (the ratio of actual air/fuel ratio to stoichiometry ratio for a given mixture) about 2 reduce the thermal load and the level of NO_X emission to meet the standard emission requirements without an additional after-treatment system [4]. Therefore, a low NO_X emission and low knock probability due to the low combustion temperature is the main advantages of the ultra-lean natural gas engine [5,6]. Natural gas has chemical properties with a high H/C ratio of around 3.7. Thus, by

changing the fuel from diesel with a ratio of 1.8 to natural gas, an immediate reduction of CO_2 is achievable. As a result, the gas engines produce less CO_2 and even 20% less than similar gasoline engines [7]. At lean equivalence ratios, like for the lean-burn spark-ignition engine, a low amount of CO can be achieved [8]. Moreover, the formation of CO emission is high primarily when the engine operates close to stoichiometric or during warm-up when the wall is cold.

Nevertheless, a major challenge in natural gas engines is the volume of methane slip [9]. Global Warming Potential (GWP) values relative to CO_2 is about 21−28 times in 100 years for methane [10]. Therefore, incorporating methane slip as a CO_2 equivalent eliminates nearly all the advantages of converting a diesel engine into a natural gas engine [11]. Moreover, a lean-burn natural gas engine has a narrow optimized operating area in a full load. A widened operating area is only in low loads with low brake mean effective pressure (BMEP), where the efficiency of the engine is also lower. For an engine working in the maritime industry, these two areas should be considered separately and individually.

To enhance the combustion and reduce the lean-burn gas engine's methane slip, redesigning the engine was suggested [12]. Since the main sources of the methane slip for this type of engine are crevice volume, quenched flame, and gas exchange process during valves overlap [13]; the improvements mainly were viewed on these sources. Stenersen and Thonstad [14] recommended two general strategies for entering into a lower amount of methane slip region:

1. Primary measures related to engine design and operation,
2. Secondary measures, i.e., exhaust gas after-treatment.

The engine redesigning involves, but is not limited to, lowering the crevice volume (dead volume) and using variable valve timing to minimize the valve overlap. The latter restricts the methane slip from the gas exchange process significantly. There are always constraints in redesigning strategies; for instance, the oil temperature should never exceed 170° Celsius. Thus, a quenched flame near the crevice volume, especially between the piston and the liner is essential [15].

Exhaust after-treatment systems have already been widely used to control the total emission of the engines. For typical gas engines with a lean mixture, palladium and platinum-based catalysts have shown a reliable performance of both methane and formaldehyde reduction [16−18]. However, such instruments' lifetime restricted the application of an after-treatment system for marine engines [14]. Wärtsilä reported acceptable methane conversion ratios in marine engines, although they also stated that the main challenge was the deactivation by sulfur [19].

In order to address the methane slip issue in marine gas engines, design modification prevailed as the only practical strategy. Installing a pre-chamber for stable combustion [14], injecting the liquid diesel fuel as the pilot with 1%−5% [20], and regulating the airflow by variable turbine geometry (VTG) [21] are proposed to heighten the engine performance and lowering the methane slip emission. Rolls Royce reported a low methane slip engine with high stability for marine applications [22]. Besides, Wärtsilä reported a decline of approximately 15% in greenhouse gas emissions using a spark-ignition gas engine. The improvement could be achieved compared to the already low emission levels of the Dual Fuel (DF) engine with the lowest total cost of ownership along with the smallest environmental footprint [23].

The influence of the methane slip reduction methods is investigated in steady-state and mostly in full loads, and the cumulative methane slip reduction is confirmed. However, a real ship works in waves with a time-varying inflow on the propeller and the engine. The engine's response during the transient load may entirely deviate from the steady condition. The consequences of imposing several sea waves with different wave amplitudes, wave frequencies, and wave directions remarked the influence of time-varying load on methane slip and NO_X formation. The flame quenching is one of the key players for extra methane slip, and the rich mixture was the main player of extra NO_X [24]. Further works are attempted to control the combustion around the full load [25]. The transient conditions analysis explained that the turbocharger's mechanical delay is the primary source of the out-of-range excess ratio. The lean combustion is sensitive to the air-fuel ratio, and any divergence from the setpoint results in further methane slips. With load drop in transient conditions, extra boost pressure is delivered to the cylinders, and the air-fuel ratio exceeds the setpoint. This additional air is the main source of quenching flame and methane slip. Multiple controlling systems were established and concluded that the closed-loop and open-loop controllers always had a time delay. A fast response solenoid valve with a proper orifice diameter fitted at the end of the intake manifold could adjust the excess air ratio and discard almost all additional methane slip. The only drawback of the proposed method was a 50% higher amount of NO_X. Retarding spark ignition timing corrected the added NO_X formation.

Part-loads operation of the engines affects the combustion stability, emission formation, and thermal efficiency [26]. Due to the non-developed flame propagation of lean mixture in a DF engine using diesel and natural gas as the fuels, indicated thermal efficiency is low. In addition, higher CO and UHC emissions deteriorate all the advantages of low emission DF engine [27]. One specific solution for the DF engine is advancing diesel injection timing to increase the pressure rise rate [28]. The effect of injection pressure on natural gas/biodiesel dual-fuel engine at a low load condition demonstrated the advancement of the combustion stability and emission reduction due to the improved pilot fuel atomization and shorter ignition delay [29].

For the lean-burn gas engines, installing a throttle for the lower load (less than 30%) was proposed [30]. The pros and cons of using throttle have already been investigated in numerous works on both CI and SI engines [31,32]. The intake-throttling device intensifies exhaust gas recirculation

(EGR) injection by decreasing the pressure behind the intake valve, and it effectively accelerates the natural gas combustion [33]. In contrast, the engine's efficiency decreases due to the pumping losses caused by the throttle's partial opening [34]. Therefore, installing a throttle valve to regulate the air ratio throughout the engine loading is refused. The influence of throttling for the lower loads during harsh weather conditions is also an issue since the load variation is usually faster than the throttle valve response [35].

The literature found the gas engine's response and the formation of emission during the transient conditions. However, they mainly focused on the full load with regular sea waves. Despite all that research, they lacks studies exploring to what extent the lean-burn gas engine can operate at low loads. The present work aimed to underline the lean-burn gas engine response and emission formation during part-loads and irregular time-varying load. The novelty of this study is showing the significance of lower loads operation on combustion stability and emission formation with a specific focus on methane slip comparing to high load operation. The irregular fluctuated loads on the propeller are according to an actual vessel journey.

The remainder of the paper is organized as follows: In section 2, the simulation methodology with a focus on flame and emission modeling is discussed. Next, the motivation and limitation of this research are presented in section 3 and 4, respectively. Afterward, in section 5, the validation of the model and the analysis of the results of the part-load operation are presented. Finally, section 6 draws the highlights of the part-load operation of gas engines and concludes the disparity between transient loading and steady-state condition.

2. Establishment of the engine model

Engine modeling is a viable solution for predicting engine thermal efficiency, fuel consumption, and emission compounds formation. The advantages of doing modeling than the on-board measurement are cost and time effectiveness, and there is the possibility of tracking the engine on a very short time scale.

Detailed modelings of the engine's fundamental elements, such as intake and exhaust manifolds, intake and exhaust valves, controllers, combustion chamber, fuel system, and turbocharger, were taken into account by mathematical equations and discretized control volume implementations in this study. All the models are implemented into the commercial GT-SUITE package. The most important part of the modeling during the transient conditions was combustion modeling. To predict the combustion progress for the SI engine, the $SI_{turbulent\ flame}$ model is proposed [36]. The model has the potential of predicting the combustion burning rate based on laminar (S_L) and turbulent (S_T) flame speed. It was assumed that there are two zones, burned and unburned zone, and the eddies of the unburned zone are entrained in the flame front at a turbulent velocity while the mixture of fuel and air is burning by laminar velocity. The rate of transformation of unburned to the burned zone is calculated by Eqs. (1) and (2):

$$\frac{dM_e}{dt} = \rho_u A_e (S_T + S_L) \tag{1}$$

$$\frac{dM_b}{dt} = \frac{M_e - M_b}{\tau} \tag{2}$$

where index b symbolizes burned classification, u unburned classification, and e entrained classification.

In order to calculate the laminar flame speed (S_L), Heywood [37] recommended Eq. (3) for several hydrocarbon fuels:

$$S_L = (B_m + B_f(\varphi - \varphi_m)^2)(\frac{T_u}{T_0})^{\alpha} (\frac{\rho}{\rho_0})^{\beta} f_{Du} \tag{3}$$

where for natural gas fuel [38]:

$$\alpha = 0.68\varphi^2 - 1.7\varphi + 3.18 \tag{4}$$

$$\beta = -0.52\varphi^2 + 1.18\varphi - 1.08 \tag{5}$$

f_{Du} is the dilution effect and is employed as:

$$f_{Du} = 1 - 0.75A(1 - (1 - 0.75A \times Du)^7) \tag{6}$$

A is a multiplier, and Du is the mass fraction of the residuals in the unburned zone.

The time constant of combustion of fuel/air mixture entrained into the flame zone (τ) was calculated by Eq. (7):

$$\tau = \frac{\lambda}{S_L} \tag{7}$$

with the Taylor length scale of:

$$\lambda = a\,(\frac{L_i}{\sqrt{Re_t}}) \tag{8}$$

and

$$Re_t = \frac{\rho_u \dot{u} L_i}{\mu_u} \tag{9}$$

and calculation of turbulent flame speed is done by Eq. (10):

$$S_T = b\dot{u}\,(1 - \frac{1}{1 + c(\frac{R_f}{L_i})^2}) \tag{10}$$

Moreover, $\dot{u}$ and L_i are turbulent intensity and turbulent length scale, respectively [39].

Calculation of A_e is presented in Ref. [40].

Since the fluid flow is essential in determining the flow dynamic delay and the turbocharger response, the equation of conservation are involved in the conservation of momentum as well as Eqs. (11) and (12) [36]. The dimensions for all the pipes and junctions are implemented based on the

designed components, and different discretized length scales for the straight pipes and bends are chosen.

In all discretized volumes, Eqs. (11) and (12) generate the mass and energy in each volume. With the available volume and mass, the density can be calculated. Afterward, the equations of state define density and energy as a function of pressure and temperature, and the solution will be continued iteratively.

$$\frac{dm}{dt} = \sum_{boundaries} \dot{m} \tag{11}$$

$$\frac{dme}{dt} = -\rho \frac{dv}{dt} + \sum_{boundaries} (\dot{m}h) - h_c A_s (T_{fluid} - T_{wall}) \tag{12}$$

$$\frac{d\dot{m}}{dt} = \frac{dpA + \sum_{boundaries}(\dot{m}u) - 4C_f \frac{\rho u|u|}{2} \frac{dxA}{D} - K_p(\frac{1}{2}\rho u|u|)A}{dx} \tag{13}$$

Pressure drop is calculated in all of the volumes, and heat transfer is also modeled. More information is given in Ref. [24].

Apart from the modeling of the components with fluid flow, there were also required to study how the actuators and control parameters influence in terms of engine stability. The main target was to keep the engine in a determined excess air ratio, and for this purpose, a closed-loop proportional-integral-derivative (PID) controller was employed on the turbine to regulate the VTG. This controller plays a dominant role in regulating the air-fuel ratio, and thus, the general response of the engine. Moreover, two other regular PI controllers (PID with a coefficient of $D = 0$) are also set a place:

- The fuel flow regulator with engine speed feedback,
- The throttle opening angle to restrict the airflow if the load is lower than 30%.

In the present study, the focus is to recognize the engine emission formation during part load where the load variation occurs in an area where the methane slip usually is higher than other conditions. For this purpose, a predictable model is used. The methodology for calculation of UHC formation and the correctness of the method is extensively described in Ref. [13]. In order to calculate the amount of total mass of unburned fuel, Eq. (14) is employed:

$$UHC = \int_{IVO}^{IVC} \dot{m}_f - \int_{comb} \dot{m}_f - \int_{post\_comb} \dot{m}_f \tag{14}$$

$\dot{m}_{f\ IVO\text{-}IVC}$ is the mass of fuel injected in the combustion chamber from intake valve opening to intake valve closing, $\dot{m}_{f\ comb}$ is the amount of fuel which is burned during the main combustion and $\dot{m}_{f\ post\text{-}comb}$ is the mass of fuel which is oxidized in post oxidation from the end of combustion to exhaust valve opening.

The post-oxidation (post-comb) of unburned fuel is based on reaction rate of R_K, according to Eq. (15).

$$R_K = 2000 A R_S e^{-\frac{1600K \times B}{T}} [f_{fuel}][f_{O_2}] \tag{15}$$

where A and B are multiplier, and T is the mass-averaged overall temperature, and R_S is the burn rate equal to dM_e/dt calculated by the combustion model of Eq. (1).

The reported value for UHC is calculated by:

$$BS_{UHC} = [\frac{\sum_{i=1}^{no.cyl}(RC \times UHC_{total})}{Power_b}][\frac{6000 N_{avg}}{n_r}] \tag{16}$$

where $Power_b$ is brake power, n_r is revolutions per cycle, 2 for a 4-stroke engine. and R_C is:

$$R_C = 1 - \frac{m_b}{m_{total}} \tag{17}$$

where m_b is the mass of burned species in the cylinder i at the start of the cycle and m_{total} is the total mass of all species in cylinder i when the exhaust valve opens.

For the formation of NO_X, Zeldovich mechanisms are being employed [41]:

$$O + N_2 = NO + N \tag{18}$$

$$N + O_2 = NO + O \tag{19}$$

$$N + OH = NO + H \tag{20}$$

where Eqs. (18) and (19) are thermal NO_X formation and Eq. (20) is particular at near-stoichiometric conditions and in fuel-rich mixtures. The reaction rate for the three mechanisms are:

$$K_1 = F_1 e^{-\frac{38000A_1}{T_b}} \tag{21}$$

$$K_2 = F_2 T_b e^{-\frac{3150A_2}{T_b}} \tag{22}$$

$$K_3 = F_3 \tag{23}$$

For Eq. (18), Eq. (19), and Eq. (20), respectively. A_1 and A_2 are constant coefficients for tuning the modeling. T_b is the burned mixture temperature.

In order to calculate the unburned and burned zone temperatures and pressure at each time step, the cylinder's contents are considered, including residual gases from the previous cycle. The amount of fuel-air mixture transferred to the burned zone is determined by the burn rate. Once the chemical equilibrium calculation is carried out for the entire burned zone, the new composition of the burned zone will be determined, and the internal energy of each species is calculated. Next, the energy of the burned zone is obtained by summation over all of the species. By applying the energy conservation equation in the chamber, the new temperatures and cylinder pressure of the unburned and burned zone are obtained.

Table 1 Model coefficients.

Item	Symbol	Value
Dilution factor	A	1
Turbulent flame speed	b	1.18
Taylor length scale	a	1
UHC multiplier		1
Crevice volume fraction		0.01
NO_X multiplier		1
Laminar flame speed	B_m	0.490
Laminar flame speed	B_f	−0.59
Laminar flame speed	φ_m	1.390
F_1		7.6e10
F_2		6.4e6
F_3		4.1e10

Table 1 provided the model coefficients being used in Eqs. (1)−(23). The schematic of all the influential components being modeled and studied in this research can be represented, as shown in Figure 1.

3. The motivation of present research

Taking the vessel journey's temporal patterns into account, Figure 2 gives a histogram of the engine loading for one month. The histogram algorithm shows that the engine load, for the most part, has two ranges of the working area, 80%−100% and 30%−60%. Modeling and analysis of the engine output, including the fuel consumption, combustion efficiency, and emission compounds for the area closed to the full load, 70%−100%, is already done [24]. Examining the performance and emission of the entire journey is difficult because of the simulation run time. Therefore, a continuous 50 min of the engine loading was separated from

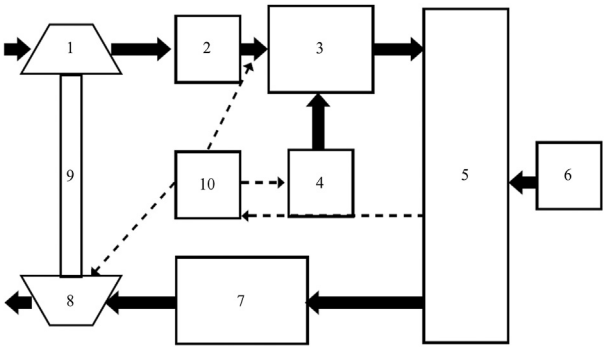

1 Compressor 2 Intercooler 3 Inlet manifold
4 Fuel 5 Block 6 Torque
7 Exhaust manifold 8 Turbine 9 Turbo shaft
10 Controllers box

Figure 1 Engine modeling schematic. The thick arrows indicate the fluid flow passage, and the dashed arrows indicate the controllers' elements, consisting of VTG, air throttle, and fuel flow by feedback from the engine speed.

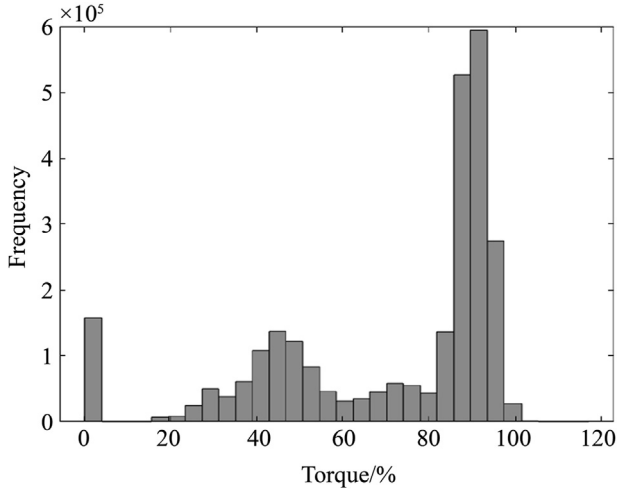

Figure 2 The torque percentage frequency of occurrence for 31 days of vessel operation in the sea.

this long vessel tour. The histogram of the loading is shown in Figure 3. This time duration has between 25% and 85% of loading and meets our requirements for examining the engine loading in part loads.

Table 2 and Table 3 represented the vessel specifications and medium-speed four-stroke natural gas engine, respectively. The vessel is a cargo vessel owned by Nor Lines and was constructed by Tsuji Heavy Industries in China, which is fitted with nine cylinders Bergen B35:40 gas engine from Rolls Royce Company.

The engine and the vessel logged data are available for the entire journey, but not for the emission data. There is no data available for the amount of methane slip, although logging the emission output during the transient conditions is not simple. The fastest instruments, such as the Flame

Table 2 Ship main specification.

Item	Value
Length between perpendiculars/m	117.6
Breadth/m	20.8
Design draft/m	5.5
Design shaft submergence/m	3.3
Service speed/kts	15

Table 3 Engine specification.

Item	Unit	Value
Number of cylinders	–	9
Cylinder bore	mm	350
Cylinder stroke	mm	400
Connecting rod	mm	810
Maximum power	kW	3940
Rated speed	rpm	750
Fuel type	–	Natural gas
IVC (BBDC)	CA	40
EVO (ATDC)	CA	130

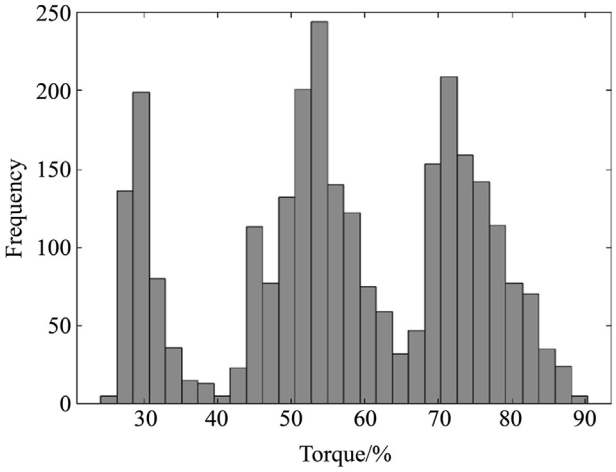

Figure 3 The torque percentage frequency of occurrence for almost 50 min of engine operation.

Ionization Detector FID sensor, have a response time and cannot measure the emission compounds in the transient loading. Air Pollution Monitor MEXA-1170HFID Series made by HORIBA is an example. The instrument has a time delay due to using sample gas analysis [42]. Therefore, modeling is essential to address the influence of time-varying load on emission formation, such as methane slip and NO_X.

Figure 4 represented the implemented torque during the time. The red dashed line shows the logged data from the vessel, and the blue line shows the imposed torque on the simulation. This satisfactory overlap confirms that the engine model followed the propeller load precisely.

4. Limitation

Generally, the concentration of the emission compounds differs in chemical equilibrium rather than the detailed chemical mechanism. Nevertheless, implementing the detailed kinetics to find the emission level during combustion and post oxidation needs considering hundreds of reactions. Therefore, the basic formation mechanism is provided for the pollutants, and this simplification neglected to address all the formation processes. In addition, the fuel may react during the combustion process and form formaldehyde [43]. In the presence of hydrocarbon compounds, a new formation of oxygenated hydrocarbon (OHC) may occur [44]. This step is also simplified in the modeling, and the only source of UHC is the amount of unburned fuel, which is presented as methane slip.

In addition, the model is not validated for CO in different loading points in steady-state. Thus, it is impossible to consider its output for transient conditions. Moreover, CO may form from incomplete combustion in a lean mixture [45] and become an important output emission of lean combustion. However, due to simplification in chemical mechanisms, this process was skipped.

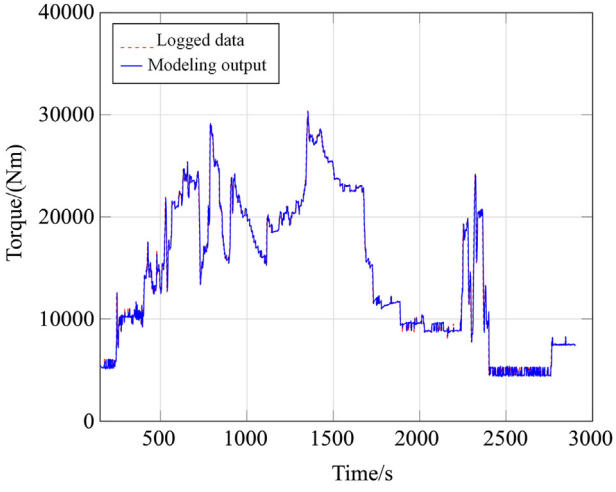

Figure 4 Implemented torque variation for almost 50 min based on the propeller torque from the vessel.

5. Results and discussion

A marine engine operates both in steady-state and transient conditions. During the steady-state, the torque and speed are almost constant; hence, the other results do not alter either. While under transient conditions, all elements are influenced by the time-varying torque, such as engine speed, fuel flow, boost pressure, airflow, intake temperature, and in-cylinder pressure. The engine speed is typically an output of the conditions, and in a marine application, it is an output of vessel speed, gear-box ratio, the pitch of the propeller, and the engine power. Since the whole propulsion system was not modeled in the simulation, the speed was given to the model as a target curve. In order to keep the speed in an appropriate range, a PID system regulated the fuel system to reach this target curve. It should be noted that this curve acts like a captain's desire to retain the vessel's velocity. The logged data, as well as the simulation output, is shown in Figure 5. It can be seen that there was a small negligible gap between the logged and the modeling data.

The fuel consumption of the engine in Figure 6 revealed an immeasurable overlap between engine logged data and modeling results. Nearly the same approach was found in Figure 7. The air pressure of the intake manifold changed from 1 bar to 2.5 bar in absolute, just with a bit more uncertainty for simulation output. Two immediate reasons for this uncertainty arises:

1. Simulation issue
2. Measuring issue

The simulation issue involves the turbocharger prediction, which does not accurately predict the load's shift, resulting in a higher or lower boost amount. This inequality may originate from the imposed look-up map or the thermodynamic equation simplification. However, looking at Figure 5 at a time of 240 s shows that the engine speed

quickly declined from 500 to nearly 430 rpm, while the logged data of fuel flow and boost pressure have not changed at this time. Since the logging occurs once each second (which means one out of six cycles for the speed of 750 rpm), a significant number of the variation is never recorded in the measuring of the output. Therefore, it can be concluded that the measuring issue is more feasible than the simulation issue.

The comparison of logged data and numerical output during various loads and speeds confirmed the model's correctness during the transient conditions and the potential of predicting the general engine outputs. Besides, the variation was observable in a shorter time scale with the modeling. However, some developments in simulation output may still be needed. For example, the boost pressure in lower loads predicts around 1.05 bar on average, while the logged data is 1.02. Although this small quantity is negligible, 3% of the additional boost may contribute to a more in-depth emission quantity.

To ensure the predictability of the emission model, the results of the steady-state, which is provided by the manufacturer, are presented in Figure 8. The results are in good agreement with the available data, and all errors between the simulated and measured outputs are within acceptable levels. Therefore, the models with the implemented tuning coefficients in steady-state for UHC and NO_X have been used for transient conditions.

The engine's part-load operation can significantly alter the amount of emission formation; thereby, methane slip and NO_X formation as the two primary emissions of lean-burn gas engines are presented in Figure 9 and Figure 10. During steady-state with a nominal load, almost 2% of fuel remains unburned, which is believed as unburned hydrocarbon emission. This quantity increases when the engine load distances from the power curve or changes in an oscillating condition. Interpretation of the results of Figure 9 states that flame propagation has an uncertainty

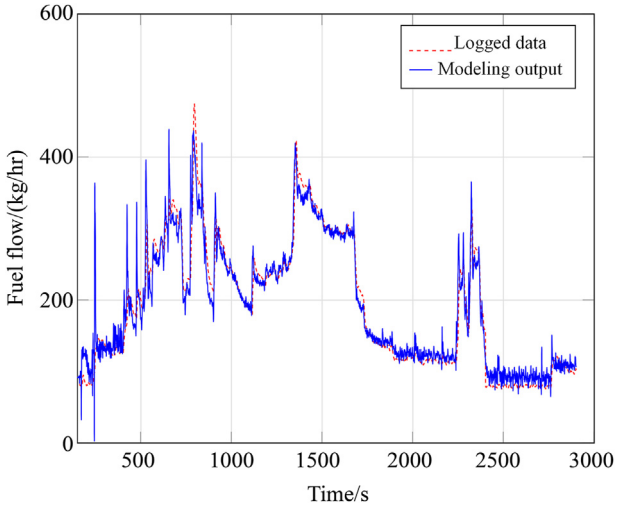

Figure 6 Fuel flow. The consumed fuel by the engine is predicted accurately throughout the transient condition.

even with a slight load shift throughout the part loads (1). This uncertainty issued a large oscillation of the UHC formation, and methane slip increased notably by several apparent variations. It is worth noting that the first 200 s can not be considered as the simulation output because the model we have implemented requires almost 160 s to reach a convergence to the values where initialized parameters.

Between 1000 and 2000 s, when speed and torque increased gradually and declined afterward, the UHC amount was not constant, but there was less change on the output (2). This stability demonstrates how the higher load plays a dominant role in providing stable combustion.

As shown from (1), the same fluctuation occurs for the area (3). As long as the load and speed are low, and the engine is working in low loads, any slight variation on propeller load results in a higher amount of methane slip.

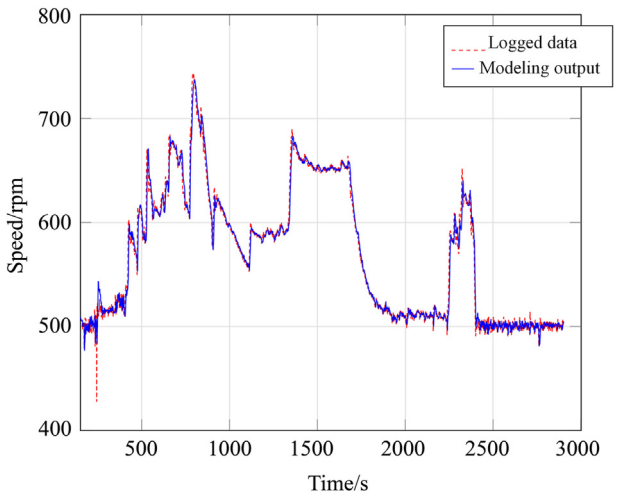

Figure 5 Engine speed. The speed varies from about 500 rpm to 730 rpm in implemented transient condition.

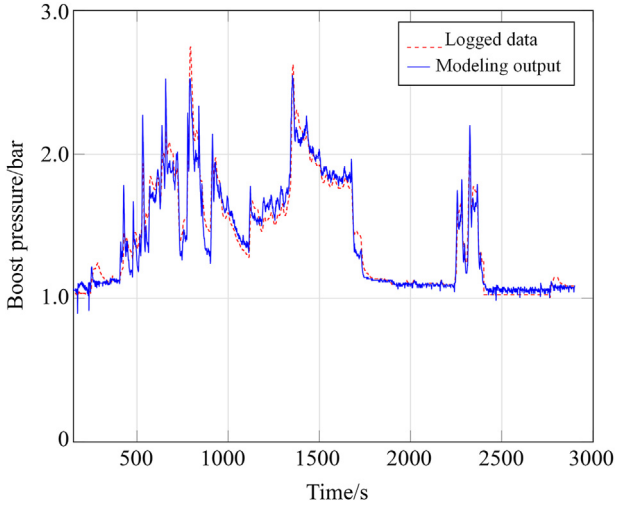

Figure 7 Boost pressure. The absolute pressure measured after the intercooler confirms the correctness of the turbocharger modeling.

Figure 10 indicates the total formation of NO_X. As can be seen, the only stable area of this compound formation is between 1200 and 1800 s. The duration is when the engine was working at 670 rpm and torque between 20,000 and 30,000 Nm. The result again confirms the improvement of the engine response in full-load in comparison with a part-load.

In the absence of quantitative airflow data, the main item for recognizing the mechanisms is the simulation output.

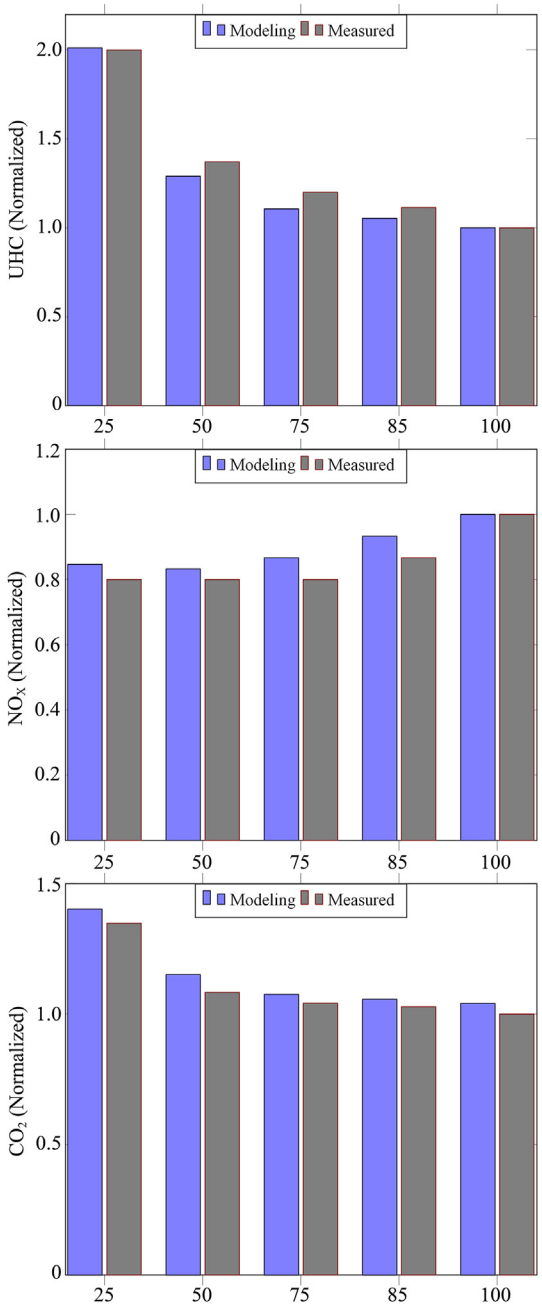

Figure 8 Comparison of measured data and engine simulation in steady-state. The *X*-axis shows the load percentage, and the *Y*-axis gives the measured-modeled output. The results are normalized by the measured value in 100% load.

All the rotating components, such as a flywheel, turbocharger shaft, and crankshaft, have a moment of inertia. During transient conditions, acceleration or de-acceleration of the rotating mass orders a different amount of energy than the other components. The larger the mass moment of inertia, the more significant the difference. For example, if the load rises, a part of the energy will accelerate the shafts to reach the new stable state. In contrast, this delay in turbochargers appears with an additional excess ratio when the load suddenly declines. This excess ratio is a function of the largeness of load variation and frequency of the propeller load. The inclination of the air-fuel ratio for the implemented load is shown in Figure 11. The ratio attempts to enter into the

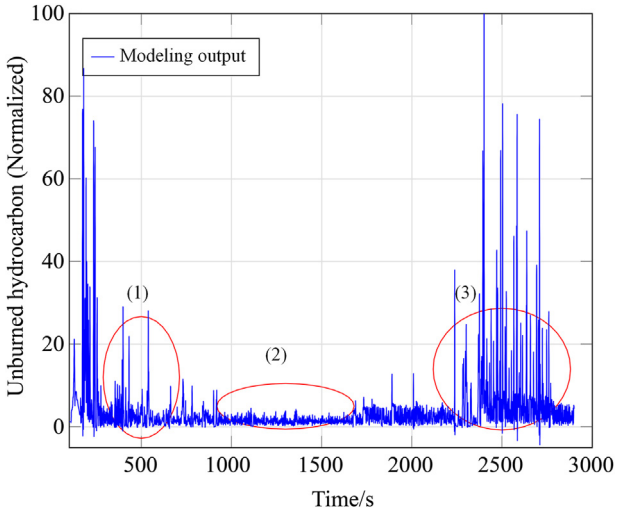

Figure 9 Methane slip. A significant variation occurs on total methane slip when the engine slightly oscillates in lower load, shown by (1) and (3).

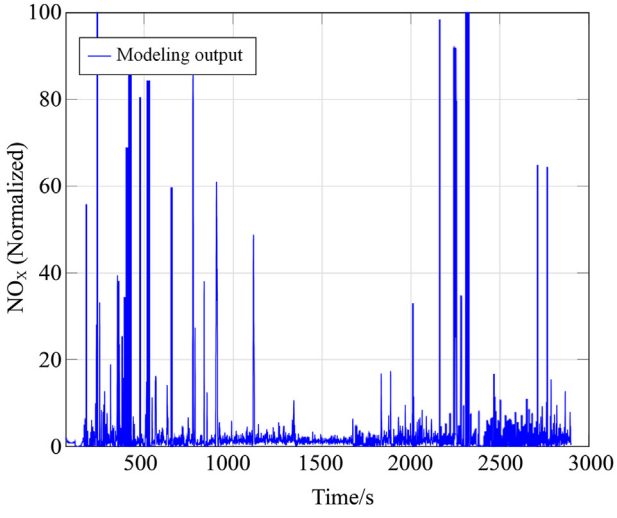

Figure 10 NO_X formation increases even when the load is lower in transient condition. An unstable combustion results in high excess air ratio in short time scales and consequently a high in-cylinder combustion temperature.

setpoint area, while the load shift prevents the stability, and the ratio fluctuates in a range of 30−32 mostly. During the higher loads, only a high fluctuation on propeller load influences the air-fuel ratio, while during part-load, striking variation occurs even with small load change.

Due to the unreadability of the data throughout the entire time, we presented the average values by the necessity of approximations.

Figure 12 and Figure 13 indicate the mean value of boost pressure and consumed fuel in various loads and speeds. Since the speed was less important than the load, the x-axis presents the load percentage. The average value of the simulation results was found good entire the loads, except the fuel flow in minimum and maximum load, where there is an almost 5% gap between the results. It must be highlighted that the load percentage was chosen in the most stable moments. For example, 71% of the load is the average of seconds from 1548 to 1675, almost 2 min, and 28.8% between 2406 and 2761, almost 6 min. Moreover, 68% of the load consumed more fuel than 70%. This contrast stems from the engine speed difference, where the power of 68% is higher than 70%.

The available emission logged data in Figure 14 and Figure 15, which was already shown in Figure 8, implies a continuous 750 rpm in several loads, while the simulation output is for a range of speed from 500 to 750 rpm. Therefore, with a rough comparison based on the load of the engine, Figures 14 and 15 are provided. The logged data of steady-state in Figure 14 determines that increasing the load contributed to the lower quantity of methane slip, and this trend is due to the developed combustion in higher loads, where the methane slip quantity declined almost linearly to half from 25% to 100%. It is worth noting that the data are normalized based on the value in 100% load; hence the values on the 100% load are equal to one. The simulation

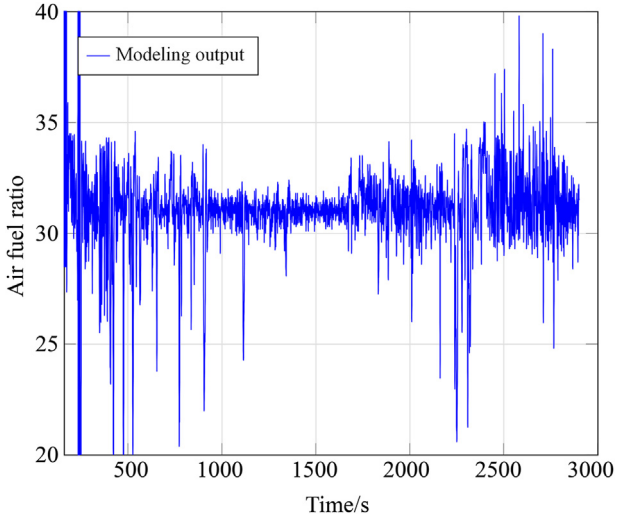

Figure 11 Air fuel ratio. The setpoint is 31, while during time varying load, the air fuel ratio fluctuates between 20 in minimum and 40 in maximum. The higher excess ratio means higher methane slip, and the lower excess ratio means higher amount of NO_X.

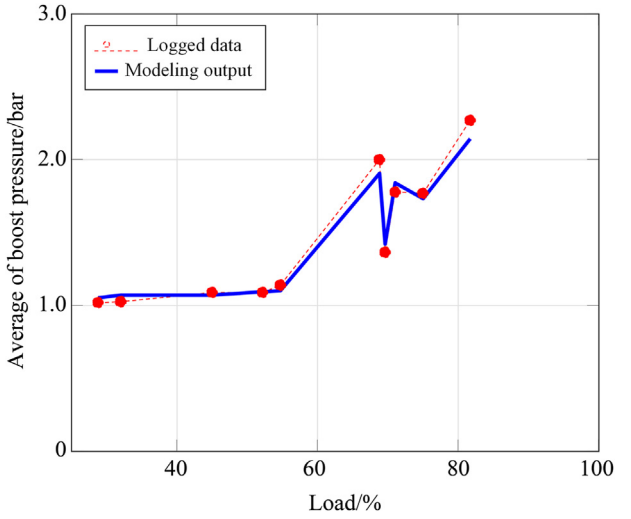

Figure 12 Average of boost pressure - a comparison of steady-state and transient conditions.

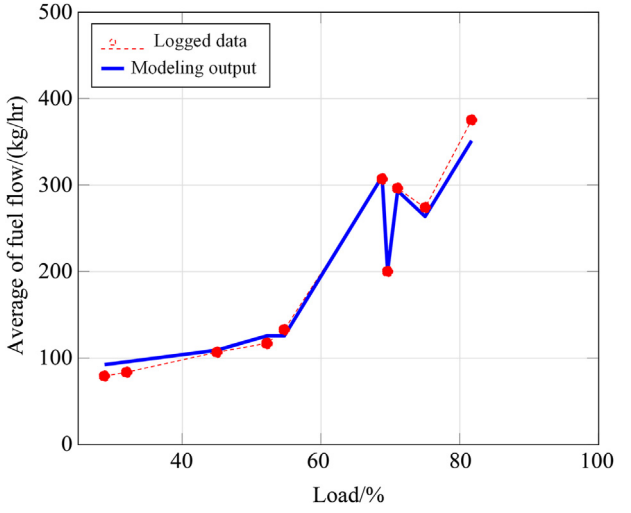

Figure 13 Average of fuel flow - a comparison of steady-state and transient conditions.

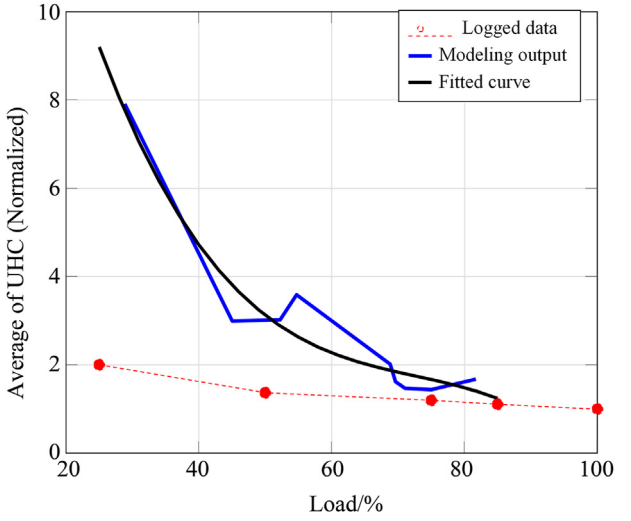

Figure 14 Average of UHC - a comparison of steady-state and transient conditions.

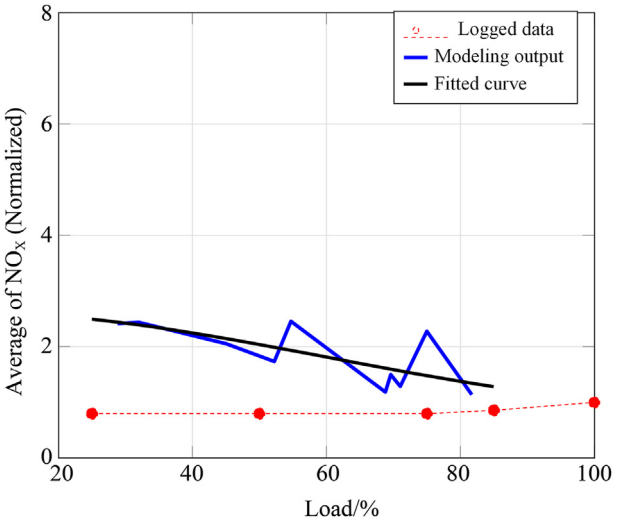

Figure 15 Average of NO_X - a comparison of steady-state and transient conditions.

output for transient conditions, however, showed a higher number. The average value with a 28% load is almost four times more than the measured data.

Comparing methane slip behavior for a different engine but installed both on-board and test-bed measurements showed almost the same output [30]. As the load becomes more than 50%, the agreement was rather good in both installations. But for the loads lower than 25%, the difference exceeded 400%. This rise in the methane slip quantity highlights the importance of keeping the marine engine load always in high loads.

Concerning Figure 15, a lower load produced a smaller quantity of NO_X during the steady-state. The reduction is 20% from full load to 25% load; however, NO_X showed a contrast procedure in the transient conditions and was increased in lower loads. This contrasting behavior can be explained again in the engine response due to the time-varying load, where the air-fuel ratio suddenly declines to a lower point than the setpoint.

In both Figures 14 and 15, a fitted curve, which explains the probable trend of the emission formation is added by using a polynomial curve fitting method in MATLAB by an order-fits of 4. It is immediately apparent that the UHC formation after 70% load is not sensitive to tiny load variation, and the value is equal to the steady-state. With an approximation, the same occurs for the NO_X emission. Furthermore, there is a linear correlation between NO_X formation and load decrease, while an exponential function can be found for UHC. Therefore, higher load variation in lower loads may increase the methane slip predominantly.

6. Conclusion

In this research, a numerical model has been developed to predict a lean-burn spark-ignition gas engine's response, such as fuel consumption, turbocharger response, and emission formation in actual transient conditions. Irregular time-varying load is implemented in the modeling to examine the emission formation of the engine during part-loads. Through this research, it is concluded that:

- The data analysis from vessel journey showed the significance of frequency of occurrence of part-load operation with a working area of 30%−60% for marine engines.
- The engine modeling accurately predicted the fuel consumption and air system performance during the time-varying load.
- The simulation output tracked and presented any variance of the data, while the logged data may not record all the fluctuations due to sampling time.
- The variation of air-fuel ratio during the transient conditions showed that the engine response is more critical in lower loads, and the excess air ratio significantly changes with small load fluctuation.
- The amount of methane slip increases in lower loads both in steady-state and in transient conditions. However, in transient conditions, the load fluctuation results in more rise in total methane slip.
- Small load fluctuation influences the amount of methane slip if the load is lower than 70%. For full load operation, the engine response is more resilient to the tiny variation.
- Despite the steady-state, NO_X formation increases during lower loads of transient conditions, and the average is higher than the steady-state.

With this high level of methane slip and NO_X from lean-burn gas engines in real transient conditions of maritime operation, this type of engine may not be classified as a clean source of energy among other fossil fuels by taking the CO_2 equivalent of methane into account. However, for developing the combustion stability and reduce the emission in low load operation, there are possible methodologies with different costs and complexity:

1. Employing a hybrid propulsion system by providing power take-off (PTO) in lower loads and power take-in (PTI) in higher loads. This system maintains the engine on optimum working area based on the power curve of the engine. The drawback is increasing the cost, complexity, and demand for larger space of the installation.
2. Adding high combustible additives such as hydrogen. The addition of hydrogen proved an increase in burn rate due to the higher flame speed of hydrogen, resulting in more stable combustion in the lean limit. The drawback is the control of the mixture to prevent any knock and maximum pressure. Moreover, the most likely challenge with hydrogen is the development of a new bunkering infrastructure and suitable monitoring of the safety of storage.

References

[1] MEPC 70/18/Add 1, ANNEX 11: Roadmap for Developing a Comprehensive IMO Strategy on Reduction of GHG Emissions from Ships, Technical Report, International Maritime Organization (IMO), 2016.

[2] H.M. Cho, B.Q. He, Spark ignition natural gas en- gines - a review, Energy Convers. Manag. 48 (2007) 608−618. URL: http://www.sciencedirect.com/science/article/pii/S0196890406001919.

[3] M. Okubo, T. Kuwahara, Chapter 5 - prospects for marine diesel engine emission control, in: M. Okubo, T. Kuwahara (Eds.), New Technologies for Emission Control in Marine Diesel Engines, Butterworth-Heinemann, 2020, pp. 211−266. URL: https://www.sciencedirect.com/science/article/pii/B9780128123072000055.

[4] M. Olofsson, L. Erlandsson, K. Willner, Enhanced emission performance and fuel efficiency for HD methane engines, technical report AVL MTC report OMT 1032, Int. Energ. Agency - Advanced Motor Fuels (2014).

[5] T. Korakianitis, A. Namasivayam, R. Crookes, Natural-gas fueled spark-ignition (SI) and compression-ignition (CI) engine performance and emissions, Prog. Energy Combust. Sci. 37 (2011) 89−112. URL: http://www.sciencedirect.com/science/article/pii/S0360128510000377.

[6] R.K. Mehra, H. Duan, R. Juknelevičius, F. Ma, J. Li, Progress in hydrogen enriched compressed natural gas (HCNG) internal combustion engines - a comprehensive review, Renew. Sustain. Energy Rev. 80 (2017) 1458−1498. URL: http://www.sciencedirect.com/science/article/pii/S1364032117306974.

[7] T. Kato, K. Saeki, H. Nishide, T. Yamada, Development of CNG fueled engine with lean burn for small size commercial van, JSAE Rev. 22 (2001) 365−368. URL: http://www.sciencedirect.com/science/article/pii/S0389430401001047.

[8] S. Rousseau, B. Lemoult, M. Tazerout, Combustion characterization of natural gas in a lean burn spark-ignition engine, Proc. Inst. Mech. Eng. - Part D J. Automob. Eng. 213 (1999) 481−489. URL: https://doi.org/10.1243/0954407991527044.

[9] P. Mello, G. Pelliza, R. Cataluña, R. da Silva, Evaluation of the maximum horsepower of vehicles converted for use with natural gas fuel, Fuel 85 (2006) 2180−2186. URL: http://www.sciencedirect.com/science/article/pii/S0016236106001165.

[10] G.G. Protocol, Global Warming Potential Values, Technical Report, the Intergovernmental Panel on Climate Change, IPCC, 2014.

[11] L. Dondero, J. Goldemberg, Environmental implications of converting light gas vehicles: the Brazilian experience, Energy Pol. 33 (2005) 1703−1708. URL: http://www.sciencedirect.com/science/article/pii/S0301421504000436.

[12] V. Aeligsy, P.M. Einang, D. Stenersen, E. Hennie, I. Valberg, LNG-fuelled engines and fuel systems for medium-speed engines in maritime applications, in: SAE International Powertrains, Fuels and Lubricants Meeting, SAE International, 2011. URL: https://doi.org/10.4271/2011-01-1998.

[13] S. Tavakoli, M.V. Jensen, E. Pedersen, J. Schramm, Unburned hydrocarbon formation in a natural gas engine under sea wave load conditions, J. Mar. Sci. Technol. 26 (2020) 128−140. URL: https://doi.org/10.1007/s00773-020-00726-5.

[14] D. Stenersen, O. Thonstad, GHG and NO_x Emissions from Gas Fuelled Engines, Technical Report OC2017 F-108-Unrestricted, SINTEF, SINTEF Ocean AS, Maritim, 2017.

[15] M. de Zwart, G. van Dijk, J. Klimstra, Methane emissions from gas engines driving combined heat and power installations, J. Integr. Environ. Sci. 9 (2012) 113−125. URL: https://doi.org/10.1080/1943815X.2012.691885.

[16] B. Torkashvand, P. Lott, D. Zengel, L. Maier, M. Hettel, J.D. Grunwaldt, O. Deutschmann, Homogeneous oxidation of light alkanes in the exhaust of turbocharged lean-burn gas engines, Chem. Eng. J. 377 (2019) 119800. URL: http://www.sciencedirect.com/science/article/pii/S1385894718316681.

[17] K. Persson, L.D. Pfefferle, W. Schwartz, A. Ersson, S.G. Jarås, Stability of palladium-based catalysts during catalytic combustion of methane: the influence of water, Appl. Catal. B Environ. 74 (2007) 242−250. URL: http://www.sciencedirect.com/science/article/pii/S0926337307000719.

[18] D. Ciuparu, E. Perkins, L. Pfefferle, In situdrftir investigation of surface hydroxyls on γ-Al_2O_3 supported PdO catalysts during methane combustion, Appl. Catal. Gen. 263 (2004) 145−153. URL: http://www.sciencedirect.com/science/article/pii/S0926860X03010263.

[19] H. Korpi, Emission reduction technologies - towards zero emissions, technical report, Wärtsilä (12.10.2018).

[20] Z. Liu, G.A. Karim, Simulation of combustion processes in gas-fuelled diesel engines, Proc. IME J. Power Energy 211 (1997) 159−169.

[21] M. Kaiadi, P. Tunestal, B. Johansson, Reducing throttle losses using variable geometry turbine (VGT) in a heavy-duty spark-ignited natural gas engine, in: SAE International Powertrains, Fuels and Lubricants Meeting, SAE International, 2011. URL: https://doi.org/10.4271/2011-01-2022.

[22] Project Guide: Bergen Engine Type B, Fuel Gas Operation, Technical Report, Bergen Engines AS, 2018.

[23] Wärtsilä 31Sg, Technical Report, Wärtsilä, 2021. URL: https://www.wartsila.com/marine/build/engines-and-generating-sets/pure-gas-engines/wartsila-31sg.

[24] S. Tavakoli, S. Saettone, S. Steen, P. Andersen, J. Schramm, E. Pedersen, Modeling and analysis of performance and emissions of marine lean-burn natural gas engine propulsion in waves, Appl. Energy 279 (2020) 115904. URL: https://www.sciencedirect.com/science/article/pii/S0306261920313696.

[25] S. Tavakoli, J. Schramm, E. Pedersen, Strategies on methane slip mitigation of spark-ignition natural gas engine during transient motion, in: Automotive Technical Papers, SAE International, 2021. URL: https://doi.org/10.4271/2021-01-5062.

[26] S.H. Quintana, E.S. Castano-Mesa, S. Marın, I.D. Bedoya, J.F. Zapata, Measurement and control of natural gas mass flow in a dual-fuel engine operating at partial load through sonic nozzles, Flow Measurement and Instrumentation 65 (2019) 187−194. URL: http://www.sciencedirect.com/science/article/pii/S0955598618302516.

[27] F.M. Felayati, Semin, B. Cahyono, R.A. Bakar, M. Birouk, Performance and emissions of natural gas/diesel dual-fuel engine at low load conditions: effect of natural gas split injection strategy, Fuel 300 (2021) 121012. URL: https://www.sciencedirect.com/science/article/pii/S0016236121008899.

[28] A. Yousefi, H. Guo, M. Birouk, B. Liko, On greenhouse gas emissions and thermal efficiency of natural gas/diesel dual-fuel engine at low load conditions: coupled effect of injector rail pressure and split injection, Appl. Energy 242 (2019) 216−231. URL: https://www.sciencedirect.com/science/article/pii/S0306261919304933.

[29] K. Ryu, Effects of pilot injection pressure on the combustion and emissions characteristics in a diesel engine using biodiesel-CNG dual fuel, Energy Convers. Manag. 76 (2013) 506−516. URL: https://www.sciencedirect.com/science/article/pii/S0196890413004640.

[30] S. Ushakov, D. Stenersen, P.M. Einang, Methane slip from gas fuelled ships: a comprehensive summary based on measurement data, J. Mar. Sci. Technol. 24 (2019) 1308−1325. URL: https://doi.org/10.1007/s00773-018-00622-z.

[31] J. Reß, C. Stürzebecher, C. Bohn, F. Märzke, R. Frase, A diesel engine model including exhaust flap, intake throttle, LP-EGR and VGT, part I: system modeling, IFAC-PapersOnLine 48 (2015) 52−59. URL: http://www.sciencedirect.com/science/article/pii/S2405896315018844.

[32] V.B. Pedrozo, I. May, T.D. Lanzanova, H. Zhao, Poten tial of internal EGR and throttled operation for low load extension of ethanol-diesel dual-fuel reactivity controlled compression ignition combustion on a heavy-duty engine, Fuel 179 (2016) 391−405. URL: http://www.sciencedirect.com/science/article/pii/S0016236116301326.

[33] J. You, Z. Liu, Z. Wang, D. Wang, Y. Xu, G. Du, X. Fu, The exhausted gas recirculation improved brake thermal efficiency and combustion characteristics under different intake throttling

conditions of a diesel/natural gas dual fuel engine at low loads, Fuel 266 (2020) 117035, https://doi.org/10.1016/j.fuel.2020.117035. URL: http://www.sciencedirect.com/science/article/pii/S0016236120300302.

[34] Y. Shiao, L.V. Dat, Efficiency improvement for an unthrottled SI engine at part load, Int. J. Automot. Technol. 13 (2012) 885−893. URL: https://doi.org/10.1007/s12239-012-0089-1.

[35] S. Tavakoli, J. Schramm, E. Pedersen, Influence of turbocharger inertia and air throttle on marine gas engine response, J. Fluid Flow Heat Mass Tran. 8 (2021) 112−123.

[36] GT-SUITE, Flow Theory Manual, Technical Report, Gamma Technologies, 2017.

[37] J.B. Heywood, Internal Combustion Engine Fundamentals, 2018.

[38] J.J. Hernandez, M. Lapuerta, C. Serrano, A. Melgar, Estimation of the laminar flame speed of producer gas from biomass gasification, Energy Fuels 19 (2005) 2172−2178.

[39] T. Morel, R. Keribar, A model for predicting spatially and time resolved convective heat transfer in bowl-in-piston combustion chambers, in: SAE International Congress and Exposition, SAE International, 1985. URL: https://doi.org/10.4271/850204.

[40] N.C. Blizard, J.C. Keck, Experimental and theoretical investigation of turbulent burning model for internal combustion engines, in: Automotive Engineering Congress and Exposition, SAE_International, 1974. URL: https://doi.org/10.4271/740191.

[41] Y.B. Zeldvich, The oxidation of nitrogen in combustion and explosions, J. Acta Physicochimica 21 (1946) 577. URL: https://ci.nii.ac.jp/naid/10006948189/en/.

[42] Compact and Affordable Heated THC Measurement System, Technical Report Printed in Japan TM-TF(SK) 23, HORIBA Automotive Test System.

[43] T. Lachaux, M.P. Musculus, In-cylinder unburned hydrocarbon visualization during low-temperature compression-ignition engine combustion using formaldehyde PLIF, Proc. Combust. Inst. 31 (2007) 2921−2929. URL: http://www.sciencedirect.com/science/article/pii/S1540748906000563.

[44] S.A. Lewis, J.M.E. Storey, B. Bunting, J.P. Szybist, Partial oxidation products and other hydrocarbon species in diesel HCCI exhaust, in: Powertrain & Fluid Systems Conference & Exhibition, SAE International, 2005. URL: https://doi.org/10.4271/2005-01-3737.

[45] V. Rapp, N. Killingsworth, P. Therkelsen, R. Evans, 4-lean-burn internal combustion engines, in: D. Dunn-Rankin, P. Therkelsen (Eds.), Lean Combustion, second ed., Academic Press, Boston, 2016, pp. 111−146. URL: https://www.sciencedirect.com/science/article/pii/B9780128045572000043.